Proceedings of the Combustion Institute 41 (2025) 105970

Contents lists available at ScienceDirect

Proceedings of the Combustion Institute

journal homepage: www.elsevier.com/locate/proci

Lewis number effects on weakly turbulent premixed Bunsen flames: A comparison between DNS and experimental investigations

Marco Herbert [a], Oussama Chaib [b], Isaac Boxx [c], Simone Hochgreb [b], Nilanjan Chakraborty [d], Markus Klein [a,*]

[a] Department of Aerospace Engineering, University of the Bundeswehr Munich, 85577 Neubiberg, Germany
[b] Engineering Department, Cambridge University, Cambridge, CB2 1PZ, United Kingdom
[c] Faculty of Mechanical Engineering, RWTH Aachen University, 52062, Aachen, Germany
[d] School of Engineering, Newcastle University, Newcastle-Upon-Tyne, NE1 7RU, United Kingdom

ARTICLE INFO

Keywords:
Methane–hydrogen blends
Direct numerical simulations (DNS)
Flame imaging
Flame instabilities

ABSTRACT

Direct numerical simulations (DNS) of laboratory-scale turbulent premixed Bunsen flames have been conducted and compared with an experimental dataset encompassing three methane–hydrogen flames with volumetric hydrogen fractions of 0%, 40% and 70%. The Bunsen flames are representative of the strict flamelet regime of combustion with low turbulence intensity, which allows for the analysis of the effects induced by the combined action of Darrieus–Landau instability and non-unity Lewis number effects. The chemical aspect of DNS is treated using irreversible one-step Arrhenius chemistry, where the effective Lewis number has been determined based on a suitable calculation of the fuel mixture Lewis number along with an appropriate blending with the oxidiser Lewis number. A comparison between 2D experimental flame imaging and 3D DNS results reveals good agreement regarding mean flame shape, flame morphology, turbulent flame wrinkling, and turbulent burning velocity. This shows that simple chemistry simulations with appropriately chosen effective Lewis numbers can accurately describe turbulent burning velocity and flame–turbulence interaction for methane–hydrogen fuel blends. Provided emissions and ignition are not within the focus of the study, this might be very useful for conducting large-scale turbulent combustion simulations or large parametric studies of carbon-free or carbon-reduced fuels, which are enablers for the transformation of the energy industry into a climate-neutral circular economy.

1. Introduction

The use of fossil fuels for primary energy production has raised concerns regarding climate change. However, the challenges of phasing out existing infrastructure are substantial [1] and it is very likely that thermochemical energy conversion will remain an important ingredient of the future energy landscape [2]. Carbon-reduced fuels, such as hydrogen or hydrogen mixtures, can help to achieve net-zero targets. However, the thermochemistry of hydrogen combustion is significantly different from that of hydrocarbon fuels because of their considerably higher burning velocity and its high diffusivity, which induces significant effects of differential diffusion of heat and species due to a non-unity Lewis number. This has notable consequences for flame stability, knocking, and flashback and has led to intensified efforts to analyse, model and understand the fundamental physics of hydrogen-enriched flames [3–5].

Insight into combustion physics can be obtained through theoretical approaches, experimental investigations, and DNS analyses. Analytical models need verification from experiment or DNS. However, even advanced experimental or DNS studies in turbulent combustion research are not free of assumptions and limitations. As a consequence, a direct comparison of experimental measurements and DNS results would be desirable. However, this is often impossible because of the scale separation between these two approaches.

The complexity of parameterising chemical kinetics ranges from a few species and reactions up to hundreds of species and thousands of reactions [6]. Such mechanisms often become unmanageable for combustion DNS. In addition, accurate thermodynamic parameters for all species, including parameterisation of pressure-dependent third-body reactions, are often not straightforward. Detailed chemical mechanisms provide a wealth of information about the flame structure, but they also give rise to ambiguity in the context of analysis [7]. Therefore,

* Corresponding author.
E-mail address: markus.klein@unibw.de (M. Klein).

https://doi.org/10.1016/j.proci.2025.105970
Received 9 July 2025; Accepted 12 October 2025
Available online 4 November 2025
1540-7489/© 2025 The Authors. Published by Elsevier Inc. on behalf of The Combustion Institute. This is an open access article under the CC BY license (http://creativecommons.org/licenses/by/4.0/).

it is impossible to choose the one correct modelling approach; instead a compromise between accuracy regarding the desired aspects of the simulation (e.g. flame speed, ignition delay time, emissions) and computational cost has to be made. Conducting simulations of turbulent, premixed, statistically planar flames using the same non-dimensional numbers, numerical schemes and computational boxes, Keil et al. [7] exemplarily estimated the carbon footprint to be 25 kg CO_2 for the simple chemistry database and 1000 kg CO_2 for detailed chemistry and transport. Although simplified combustion chemistry cannot be used to predict ignition delay times or pollutant formation, there is considerable evidence that the essential aspects of the turbulence–chemistry interaction can be captured quite accurately ([7] and references therein). Simplified combustion models enable parametric studies [8] and larger computational domains, helping to bridge the gap between DNS and experiments. It is also important to consider that High-Performance Computing (HPC) consumes significant energy and contributes to greenhouse gas emissions [7], making the method selection critical. This study uses a one-step irreversible Arrhenius model. Since high-hydrogen content fuels exhibit non-unity Lewis number effects, selecting an appropriate effective Lewis number is essential for comparison with experiments. However, defining a characteristic Lewis number is complex, and the existing literature reports different approaches. For example, the characteristic Lewis number of a premixed combustion process can be evaluated by the Lewis number of deficient species [9] but this leads to a discontinuity at stoichiometric conditions. Bechthold and Matalon [10] suggested a weighting of the fuel and oxidiser Lewis number but its usage for fuel mixtures [11] needs additional treatment [12]. This approach was adopted for the current analysis.

The objective of the present work is to perform a simple chemistry DNS of a laboratory-scale methane–hydrogen Bunsen burner flame as well as a quantitative comparison between DNS and experiment. The current analysis addresses the assessment of (i) the capability to predict flame surface area and turbulent burning velocity in a laboratory-scale configuration utilising an effective Lewis number in the context of single-step chemistry, (ii) the quality of the quantitative agreement between simple chemistry DNS and experiments of hydrogen-enriched flames, (iii) the quality of agreement between 3D DNS results with the corresponding 2D flame measurements.

2. Experimental database

The experimental conditions were explicitly designed to allow a direct comparison with DNS data, which comprise identical characteristic parameters such as Damköhler $Da = lS_L/u'\delta_{th}$ and Karlovitz number $Ka = (u'/S_L)^{3/2}(l/\delta_{th})^{-1/2}$ but in particular also the dimensions of the burner, i.e. the nozzle diameter with $D = 15$ mm. In these definitions u' is the mean turbulent velocity fluctuation, l is taken to be the longitudinal integral length scale, $\delta_{th} = (T_{ad} - T_0)/max|\nabla T|_L$ is the thermal flame thickness with T, T_0 and T_{ad} being the dimensional temperature, unburned gas, and adiabatic flame temperature, respectively and S_L is the unstretched laminar burning velocity.

The experiment was conducted for the DLR premixed Bunsen Burner configuration shown in Fig. 1 for three different equivalence ratios, obtained by hydrogen enrichment of methane according to the numbers given in Table 1. A 100% H_2 case was unstable due to flashback and thus was not considered. The values presented for S_L, T_{ad} and δ_{th} have been obtained using the GRI Mech 3.0 [13]. Turbulence is generated using a high-blockage perforated plate [14], as sketched in Fig. 1.

The flame visualisation has been carried out using OH-Planar Laser Induced Fluorescence (PLIF) measurements, which yielded images with a spatial resolution of $5.7px/\delta_{th}$; Interested readers are referred to Ref. [14] for further information regarding the experiment and the measurement techniques involved. The PLIF images were processed using Filtered Canny and edge linking [15,16] algorithms, which yielded binarised flame images of the flame front comparable to the $c \approx 0.8$ isosurface according to laminar flame simulations. A total of 19300 OH-PLIF images have been binarised and processed for each experimental condition. In analogy to earlier simulation work [17–20], the parameters were chosen to maintain an inflow velocity U_0 to laminar burning velocity ratio of roughly $U_0/S_L \approx 6$, resulting in a compact flame (hence computational domain) and an integral longitudinal length scale to nozzle diameter ratio of $l/D = 1/5$. The normalised turbulence intensity attains values of about $u'/S_L = 0.68$ and was chosen in order to investigate non-unity Lewis number effects (NLE) at low turbulence intensities, often alternatively referred to as thermodiffusive instability (TDI). As the definition and onset of TDI are not uniquely defined in the literature, we refer to NLE in the following, except for places where the terminology is consistent with the literature. The aforementioned values closely approximate the measured and simulated experimental conditions [14].

Table 1
Experimental conditions (hydrogen content by volume).

Case	ϕ	H_2[%]	S_L [m/s]	T_{ad} [K]	δ_{th} [mm]
A	1.0	0	0.365	2229	0.406
B	0.8	40	0.366	2026	0.411
C	0.65	70	0.345	1818	0.447

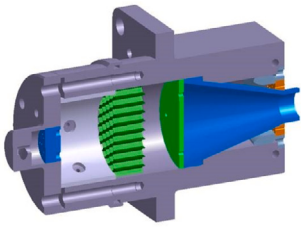

Fig. 1. Sketch of the experimental burner geometry.

3. DNS database

A fully compressible 3D DNS code SENGA [17,19] has been used for carrying out the Bunsen flame simulations, where the governing equations for mass, momentum, energy, and species are solved in a non-dimensional form. The code employs a high-order finite-difference (i.e., 10th order central difference scheme for internal points and the order decreases gradually towards a one-sided 2nd order scheme at the non-periodic boundary) for the spatial discretisation and a low storage 3rd order explicit Runge–Kutta scheme for time integration. The computational domain is taken to be a cube with side length $2D$, which equals approximately $75\delta_{th}$, and has been discretised with a Cartesian mesh of dimension 750^3. This provides a resolution of approximately $\delta_{th}/\Delta \approx 10$ as well as $\eta/\Delta \approx 11$, where η denotes the Kolmogorov scale and Δ is the DNS grid size. All boundaries apart from the inlet are specified as partially non-reflecting with standard Navier–Stokes Characteristic Boundary Conditions (NSCBC) methodology [21]. A hyperbolic-like mean velocity profile is used at the inlet face with superimposed pseudo-turbulent velocity fluctuations [18,22] matching the experimental conditions. The reacting scalars have been initialised using an unstrained laminar flame solution expressed as a function of radial distance from the centre of the nozzle. It is worth mentioning that the DNS simulations start at the outlet of the burner shown in Fig. 1 and the burner geometry is not included in the computations. Using the inlet values $u'/S_L = 0.68$ and $l/\delta_{th} = 7.46$ yield a Damköhler number of $Da = 10.94$ and Karlovitz number of $Ka = 0.21$, which are identical for all cases. A single-step Arrhenius-type chemical mechanism is employed for the computational economy. Standard values are used for the Prandtl number, $Pr = 0.7$ and the ratio of specific heats, $\gamma = 1.4$. Although the heat release parameter

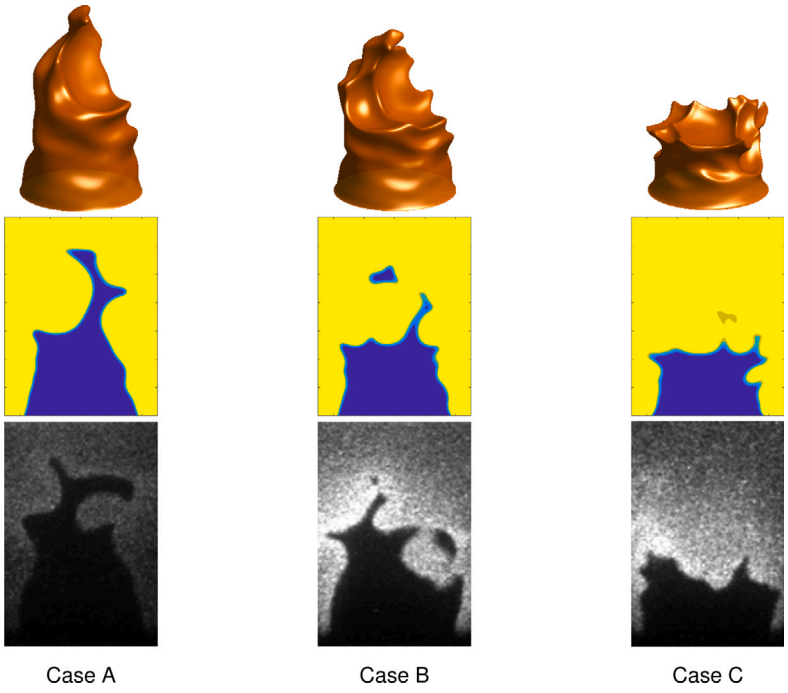

Fig. 2. Instantaneous snapshots of $c = 0.8$ isosurfaces obtained by DNS (top), flame contours from DNS (middle) and experiment (bottom) for cases A–C.

decreases slightly with increasing hydrogen content, it has been kept constant at a value of $\tau = (T_{ad} - T_0)/T_0 = 6.5$ for the sake of simplicity. The reaction rate parameters have been adjusted to match the correct laminar burning velocity. The effect of hydrogen dilution has been captured in the simple chemistry simulation by imposing an effective Lewis number (i.e. the ratio of thermal diffusivity to mass diffusivity). The effective Lewis number from the experiment has been estimated following Bechthold and Matalon [10],

$$Le_{eff} = 1 + \frac{(Le_O - 1) + (Le_F - 1)A}{1 + A}\,, \tag{1}$$

where for lean mixtures $A = 1 + \beta(\phi^{-1} - 1)$, while Le_F and Le_O denote the fuel and oxidiser Lewis numbers, ϕ is the equivalence ratio and the Zeldovich number has been set to $\beta = 6.0$ corresponding approximately to the data reported in [23,24] for hydrogen and methane flames. The fuel Lewis number, Le_F has been calculated according to the expression suggested by Dinkelacker et al. [12]

$$Le_F^{-1} = x_{\mathrm{CH_4}}/Le_{\mathrm{CH_4}} + x_{\mathrm{H_2}}/Le_{\mathrm{H_2}}\,, \tag{2}$$

resulting in $Le_{eff} = 1.04, 0.75, 0.61$ for cases A–C, respectively. The most appropriate approach to determine the effective Lewis number from experiment was not known a priori. Therefore, the Lewis numbers for DNS have initially been estimated as $Le_{eff} = 1.0, 0.8, 0.6$, which are in close agreement with the aforementioned approach. The species Lewis numbers have been determined for each case individually by a Cantera simulation, taking the unburned gas values. Fig. 2 provides a comparison of instantaneous snapshots obtained from experiment and simulation for all cases, indicating a reasonable qualitative agreement. It is worth mentioning that Bouvet et al. [11] discussed other options for estimating the fuel Lewis number, but the values obtained were too high to yield reasonable agreement in the context of the present DNS framework. For example, volumetric averaging of the fuel Lewis number yields values of $Le_{eff} = 1.04, 0.91, 0.75$ for Cases A–C, respectively. Notably, this positions Case C very close to Case B. Mass-weighted averaging gives a quantitatively wrong trend.

Determination of the turbulent burning velocity

$$S_T = \int_V \dot{\omega}_c dV/(\rho_0 A_L) \tag{3}$$

requires the calculation of the mean flame area A_L and hence the mean flame contour. This requires rather long averaging times, because the data can only be averaged in time and circumferential direction. Therefore, simulations have been run for at least 10 flow through times (i.e.,$10t_{FT} = 10L_{domain}/U_0$) after reaching a statistically steady state in order to collect a sufficient number of samples, consuming about 10^6 core hours per case.

4. Results and discussion

Fig. 2 (top row) shows an increased tendency of formation of sharply negatively curved cusps with increasing hydrogen content (i.e., from case A to case C) caused by NLE. In both simulation and experiment the flame shortens owing to a higher overall volumetric burning rate. Fig. 2 (middle and bottom rows) shows instantaneous 2D snapshots in the mid-plane of the methane–hydrogen Bunsen flames with hydrogen content of 0%, 40%, and 70% from left to right. The isocontours of the DNS represent the distribution of the reaction progress variable while in the experiment the flame has been visualised using OH-PLIF. Despite the instantaneous nature of the snapshots, there are apparent similarities between the simulation and experiment: the flame height is comparable and decreases with increasing hydrogen content and in addition the flame surface morphology from the simulation closely resembles that from the experiment, showing increasing small-scale wrinkling with decreasing Lewis number. Fig. 3 depicts the mean progress variable from DNS (dotted line) and experiment (solid line) for cases A–C. Although the simulation data still contain some statistical noise, the quantitative agreement with the experiment is very good, showing the matching flame contours, the correct flame length, and the flattening of the flame tip with decreasing Lewis number for all mean reaction progress variable contours $\bar{c} = 0.1 \ldots, 0.9$. It is important to mention that the axial offset of the experimental data in Fig. 2 is the result of a laser cut-off in order to avoid the laser beam hitting the solid parts of the nozzle. A quantitative comparison is complicated by the fact that the DNS data have nearly twice the resolution of the experimental data and that the latter is binarised while the DNS data represents a smooth transition of reaction progress from the unburned gas (i.e., $c = 0$) to the burned gas (i.e., $c = 1$). For a direct comparison

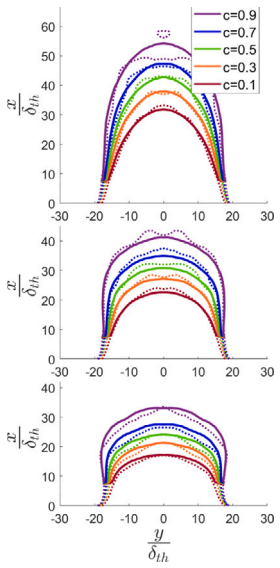

Fig. 3. Mean progress variable contours from DNS (dotted line) and experiment (solid line) for cases A (top) - C (bottom).

of the data, it is desirable to use the same postprocessing methodology. In DNS studies, the flame curvature is usually calculated as $\kappa = 1/2\,\nabla \cdot (-\nabla c/|\nabla c|)$ such that the positive curvature is convex towards the reactants. For consistency, the DNS curvature PDFs have also been obtained from 2D projections for the $c = 0.8$ reaction progress variable surface. Fig. 4 shows that the curvature PDFs become increasingly skewed towards negative curvature with decreasing Lewis number. As a result of the widening of the curvature PDFs, the peak value decreases and, consistently between DNS and experiment, shifts from about zero towards positive curvature values. It is worth noting that the mean flame contour of a Bunsen flame has a negative curvature. Hence, the fact that the most likely value of flame curvature assumes small positive values reflects the occurrence of large positively curved bulges (see Figs. 1 and 2), whereas the increasingly negative tail of the curvature PDF is characteristic of sharp negatively curved cusps. Negative skewness can be characteristic of the action of Huygens propagation [17,25] but in particular for the action of flame instabilities and NLE [17,20,26]. While all these trends are consistent between experiments and DNS, it has to be admitted that some quantitative differences remain. Because the simulations provide nearly twofold higher spatial resolution and are free of measurement noise, they are expected to resolve large-magnitude (negative) curvature more accurately. Since the probability density functions (PDFs) are normalised, differences in the tails may have some influence on the overall distribution.

It will be interesting to compare the 2D curvature distributions from Fig. 4 with 3D distributions obtained in the DNS, which are shown in Fig. 5(a). It can be observed that the 2D curvature PDFs are characterised by higher peaks and narrower distributions compared to their 3D counterparts. Based on the assumption of the isotropic distribution of the angle between the flame normal vector and the measurement plane and statistical independence of various angles and two-dimensional curvature, Chakraborty et al. [27] suggested a transformation to approximate 3D curvature PDF based on 2D measurements as $PDF(\kappa) = PDF(\kappa_{2D} \times \pi/2)$. It was also suggested that for flames with a mean flame curvature, the correction should be applied to the fluctuating part of curvature κ', because the mean flame geometry might violate the assumption of isotropy. The resulting curves are shown in Fig. 5(b), demonstrating satisfactory agreement with the theory put forward in [27]. The performance of the suggested correction deteriorates from case A to case C, presumably because the increasing effects of heat release degrade the isotropic assumption with decreasing Lewis number. Fig. 5(c) illustrates that the correction $PDF(\kappa) = PDF(\kappa_{2D} \times \pi/2)$ could be also applied to κ instead of κ' without a major loss of accuracy (compare subfigures b) and c)) when the mean radius for the investigated configuration is sufficiently high.

The analysis of flame instabilities has been pioneered by Matalon and Matkowsky [28], among others and thoroughly reviewed by Lipatnikov and Chomiak [29]. According to the analytical theory by Matalon and Matkowsky [28] the growth rate of a disturbance σ with wavenumber $k = 2\pi/\lambda$ (where λ is the wavelength of disturbance) is given as: $\sigma = S_L(\Psi_0 k - \delta_Z \Psi_1 k^2)$. The term associated with Ψ_0 is linked to the Darrieus–Landau instability, whereas the term with $\Psi_1 \propto (Le_{eff} - 1)$ is linked to thermodiffusive instability. Thus, the growth rate of the disturbance σ depends on the competition between Darrieus–Landau instability (expressed by term Ψ_0) and TDI effects (term Ψ_1) and the maximum growth rate σ_m is given by $\sigma_m = S_L/\delta_Z \cdot \Psi_0^2/\Psi_1$ (δ_Z denoting the Zeldovich flame thickness). The Darrieus–Landau instability (DLI) becomes effective when the hydrodynamic length scale of the flow becomes larger than the critical wavelength λ_c given by $2\pi/k_c$ with $k_c = 1/\delta_Z\,\Psi_0/\Psi_1$, which for the DNS cases in this work is given by $\lambda_c \approx D/3, D/4.3$ and $D/13.3$ for cases A–C. This shows the possibility of a weak DLI effect for case A. For increasingly smaller Lewis numbers the TDI effect, which competes with the DLI, becomes stronger. Finally, when the so-called critical Lewis number Le_c is reached, the term Ψ_1 approaches zero and the maximum growth rate rises sharply together with the corresponding wavenumber given by $k_m = 0.5k_c$ [20,28]. It is noted that once Ψ_1 becomes negative for $Le_{eff} < Le_c$, all wavenumbers become unstable as a consequence. A laminar premixed flame becomes unconditionally thermodiffusively unstable for $Le_{eff} < Le_c$. Both effects together are responsible for the occurrence of increasingly smaller flame structures observed with decreasing Le_{eff}. For the present DNS thermochemistry, the critical Lewis number is $Le_c = 0.54$, which should be considered a rough estimate only. This shows that the effective Lewis number approaches the critical Lewis number from case A to case C while remaining slightly greater.

It is known from analytical, experimental, and computational studies that flame instabilities and NLE may result in an enhancement of turbulent burning velocity S_T which is a fundamental quantity for modelling turbulent premixed combustion. However, to date, most of the turbulent burning velocity parameterisations have been proposed for unity Lewis number conditions and therefore disregard the effects of differential diffusion. Damköhler's hypothesis associates the increase of the rate of burning with the increase in flame area. Deviations from the hypothesis can be considered using the deviation of the ratio R, defined in Eq. (4), from unity.

$$\frac{S_T}{S_L} = \frac{A_T}{A_L} \iff R = \frac{S_T/S_L}{A_T/A_L} \approx 1 \tag{4}$$

It is well-known that Damköhler's first hypothesis does not hold for non-unity Lewis number fuels or flames with a curved mean flame contour [19,30,31]. For the assessment of the DNS capability to predict the global flame propagation, it is therefore beneficial to quantify the extent of deviation from Eq. (4) from both experiment and DNS. However, the OH-PLIF data can only be used to extract the flame length (i.e. flame area projected onto 2D) of the instantaneous and mean flame contour. Hence, for comparison, the flame edge has been extracted from DNS data ($\overline{c} = 0.5$ for the mean contour and $c = 0.8$ for the instantaneous flame surfaces) and the interface length is computed by summing Δ contributions for edge connectivity and $\sqrt{2}\Delta$ for connectivity across corners. This provided the most consistent comparison among the different options. The ratio of turbulent to laminar flame length is shown in Fig. 6 and the same qualitative trends and close quantitative agreement can be observed between the experiment and DNS with slightly larger values obtained in the case of the experiment. It should be noted that the lower part of the DNS data, corresponding to the part unavailable from the experiment, has been discarded for this evaluation. The turbulent burning velocity from DNS is given by

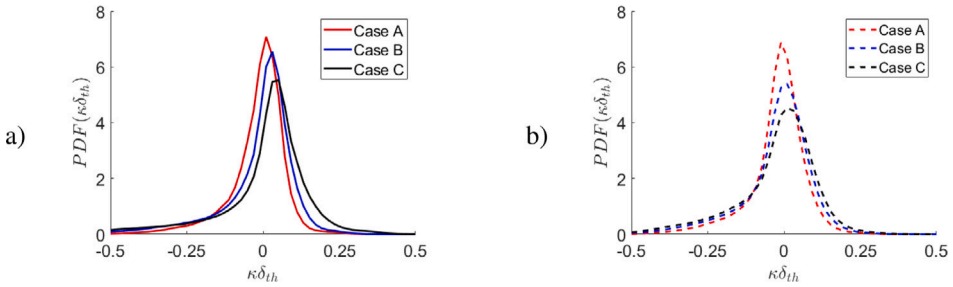

Fig. 4. (a) PDFs of curvature evaluated in 2D from simulation and (b) experiment for the $c = 0.8$ isosurface.

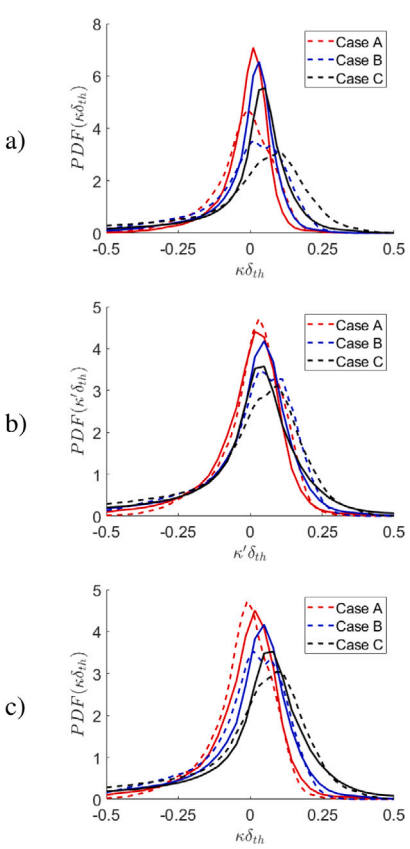

Fig. 5. (a) Comparison of 2D (solid lines) and 3D (dashed lines) DNS-based curvature PDFs for cases A, B, C; (b) Comparison of 3D PDFs of curvature fluctuation (dashed lines) with corrected 2D PDFs (solid lines) according to $PDF(\kappa') = PDF(\kappa'_{2D} \times \pi/2)$; (c) Same as (b) but using κ and κ_{2D} instead of κ' and κ'_{2D}. Results are shown for the $c = 0.8$ isosurface.

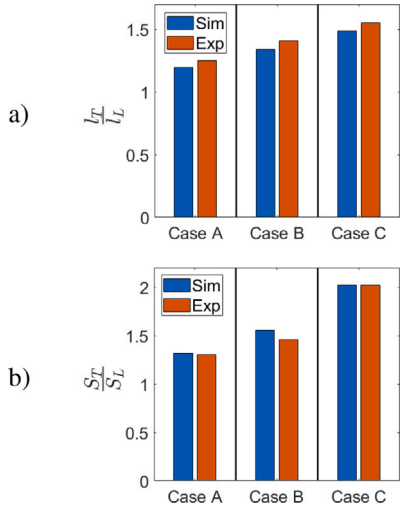

Fig. 6. (a) Turbulent versus laminar flame length l_T/l_L and (b) burning velocity S_T/S_L.

Eq. (3) while in the experiment it is typically evaluated using the mass flow rate $S_T/S_L = \dot{m}/(\rho_0 S_L A_L)$, which for the DNS results in this work yields very similar results (maximum difference 3.5%) as that of the value based on the volume integral of reaction rate. The average flame area A_L (not to be confused with the area of the laminar flame) can be determined by revolving the mean flame contour. The comparison once more yields a very close match between experimental and DNS data. The deviation from Damköhler's first hypothesis has been evaluated from the 3D DNS data using the conventional definition for turbulent flame area $A_T = \int_V |\nabla c| dV$. The ratio R increases from values slightly larger than unity, i.e. 1.05 for Case A, to 1.13 for Case B and 1.38 for Case C. Given the good agreement in terms of the 2D data (i.e. l_T/l_L and S_T/S_L), a very similar behaviour could be anticipated from the experiment in 3D.

The l_T/l_L values shown in Fig. 6 provide a measure of flame wrinkling, which is often modelled based on fractal theory [30,32]. In experimental analyses, the fractal dimension of the premixed flame surface is usually evaluated based on 2D flame surface visualisations, henceforth denoted as D_{2F}. According to Mandelbrot's additive rule [33] the actual fractal dimension D_{3F} in 3D can be obtained by $D_{3F} = D_{2F} + 1.0$ based on the assumption of isotropic self-similarity of the fractal surface. The validity of this assumption has recently been demonstrated [32] for a wide range of Karlovitz numbers based on a DNS database of unity Lewis number flames and the validity of this assumption for non-unity Lewis number flames of the present database can be seen from Fig. 7, where the correlation dimension methodology has been used to extract the fractal dimension [32] from both experiment and DNS. It is worth noting that the correlation dimension methodology for extracting fractal dimension relies upon binarised fields and hence is well-suited for both experimental and DNS data analysis. It can also be seen from Fig. 7 that the estimated fractal dimensions from the experimental measurements using Mandelbrot's additive rule are in excellent agreement with the corresponding DNS data.

5. Summary and conclusions

DNS simulations of a laboratory-scale methane–hydrogen Bunsen flame database have been conducted using a one-step irreversible Arrhenius-type chemistry treatment. The experimental database consists of three flames with volumetric hydrogen fractions of 0%, 40%, and 70% and has been specifically designed for comparison with DNS. It is shown that calculating the fuel Lewis number following the approach suggested by [12] combined with the blending of the oxidiser Lewis number, as suggested by [10], provides effective Lewis numbers

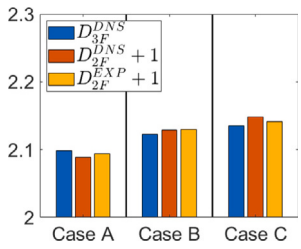

Fig. 7. Fractal dimension D_{3F} evaluated from 3D DNS as well as from 2D DNS and experimental contours using Mandelbrot's additive rule.

that enable accurate predictions of flame propagation, turbulence–chemistry interaction and non-unity Lewis number effects in comparison to 2D experimental data. The increase in turbulent burning velocity with increasing hydrogen content (i.e. decreasing Lewis number) is in close agreement with experimental data. In addition, there is very good qualitative agreement between the 2D curvature PDFs from experiment and simulation, indicating similar flame morphologies. Finally, the validity of Mandelbrot's additive rule, relating 2D and 3D fractal dimensions, has been confirmed for the present database. Nevertheless, some minor quantitative discrepancies remain for all results presented in this work. Possible reasons for these disagreements originate from the different nature of the data requiring different postprocessing steps, and approximations in terms of inlet conditions or selection of the Arrhenius parameters. As the simplification of chemistry could potentially contribute to this as well, future work needs to show whether detailed chemistry simulations would result in more accurate predictions. The value of simple chemistry simulations lies not only in the fact that this approach considerably reduces the computational time, but also in the reduction of the greenhouse gas emissions of the simulation itself.

Novelty and significance statement

The novelty of this paper lies in the quantitative comparison between laboratory-scale 3D Direct Numerical Simulations (DNS) and 2D experimental diagnostics of weakly turbulent, hydrogen-enriched methane Bunsen flames. By carefully matching inflow conditions and flame parameters, the study validates DNS against experimental results in the context of intrinsic flame instabilities. The use of a simplified one-step chemical model, coupled with a properly chosen effective Lewis number formulation enables accurate replication of flame–turbulence interaction, flame morphology, and turbulent burning velocity across varying hydrogen concentrations. Finally, the paper addresses the question how 2D optical measurements can be compared to 3D simulation data.

The work is significant because it validates DNS modelling strategies that are computationally affordable and environmentally conscious, yet robust enough for exploring flame instabilities and turbulence–chemistry interactions. It provides a framework for future high-fidelity simulations of carbon-neutral fuels, supporting scalable parametric studies critical to energy transition technologies.

CRediT authorship contribution statement

Marco Herbert: Writing – original draft, Software, Methodology, Formal analysis. **Oussama Chaib:** Writing – review & editing, Formal analysis. **Isaac Boxx:** Writing – review & editing, Data curation. **Simone Hochgreb:** Writing – review & editing, Formal analysis. **Nilanjan Chakraborty:** Writing – review & editing, Supervision, Conceptualization. **Markus Klein:** Writing – original draft, Supervision, Methodology, Funding acquisition, Conceptualization.

Declaration of competing interest

The authors declare that they have no known competing financial interests or personal relationships that could have appeared to influence the work reported in this paper.

Acknowledgements

MK and MH have been funded by dtec.bw - Digitalization and Technology Research Center of the Bundeswehr; dtec.bw is funded by the European Union - NextGenerationEU. NC is grateful to EPSRC, United Kingdom (EP/W026686/1) for financial support. IB has received funding from the European Research Council (ERC) under the European Union's Horizon 2020 research and innovation programme (Grant Agreement No. 682383). OC is supported by an EPSRC DTP Studentship (EP/T517847/1-2598182, University of Cambridge, United Kingdom).

References

[1] K. Kohse-Hoeinghaus, Combustion in the future: The importance of chemistry, Proc. Combust. Inst. 38 (1) (2021) 1–56.
[2] A. Dreizler, H. Pitsch, V. Scherer, C. Schulz, J. Janicka, The role of combustion science and technology in low and zero impact energy transformation processes, Appl. Energy Combust. Sci. 7 (2021) 100040.
[3] C. Tang, Y. Zhang, Z. Huang, Progress in combustion investigations of hydrogen enriched hydrocarbons, Renew. Sustain. Energy Rev. 30 (2014) 195–216.
[4] I. Chterev, I. Boxx, Effect of hydrogen enrichment on the dynamics of a lean technically premixed elevated pressure flame, Combust. Flame 225 (2021) 149–159.
[5] K. Whitty, H. Zhang, E. Eddings, Emissions from syngas combustion, Combust. Sci. Technol. 180 (6) (2008) 1117–1136.
[6] E. Hu, X. Li, X. Meng, Y. Chen, Y. Cheng, Y. Xie, Z. Huang, Laminar flame speeds and ignition delay times of methane-air mixtures at elevated temperatures and pressures, Fuel 158 (2015) 1–10.
[7] F.B. Keil, M. Amzehnhoff, U. Ahmed, N. Chakraborty, M. Klein, Comparison of flame propagation statistics extracted from direct numerical simulation based on simple and detailed chemistry - part 1: Fundamental flame turbulence interaction, Energies 14 (17) (2021) 5548.
[8] V.A. Sabelnikov, R. Yu, A.N. Lipatnikov, Thin reaction zones in constant-density turbulent flows at low damköhler numbers: Theory and simulations, Phys. Fluids 31 (5) (2019) 055104, http://dx.doi.org/10.1063/1.5090192.
[9] M. Mizomoto, Y. Asaka, S. Ikai, C. Law, Effects of preferential diffusion on the burning intensity of curved flames, Symp. (Int.) Combust. 20 (1) (1985) 1933–1939, Twentieth Symposium (International) on Combustion.
[10] J. Bechtold, M. Matalon, The dependence of the markstein length on stoichiometry, Combust. Flame 127 (1) (2001) 1906–1913.
[11] N. Bouvet, F. Halter, C. Chauveau, Y. Yoon, On the effective Lewis number formulations for lean hydrogen/hydrocarbon/air mixtures, Int. J. Hydrog. Energy 38 (14) (2013) 5949–5960.
[12] F. Dinkelacker, B. Manickam, S. Muppala, Modelling and simulation of lean premixed turbulent methane/hydrogen/air flames with an effective Lewis number approach, Combust. Flame 158 (9) (2011) 1742–1749.
[13] G.P. Smith, D.M. Golden, M. Frenklach, N.W. Moriarty, B. Eiteneer, M. Goldenberg, C.T. Bowman, R.K. Hanson, S. Song, W.C. Gardiner, J.V.V. Lissianski, Z. Qin, GRI-MECH 3.0, 2003.
[14] J. Pareja, T. Lipkowicz, E. Inanc, C. Carter, A. Kempf, I. Boxx, An experimental/numerical investigation of non-reacting turbulent flow in a piloted premixed bunsen burner, Exp. Fluids 63 (2022) 33.
[15] O. Chaib, Y. Zheng, S. Hochgreb, I. Boxx, Hybrid algorithm for the detection of turbulent flame fronts, Exp. Fluids 64 (2023) 104.
[16] O. Chaib, S. Hochgreb, I. Boxx, An experimental marker of thermo-diffusive instability in hydrogen-enriched flames, Proc. Combust. Inst. 40 (1) (2024) 105763.
[17] M. Klein, H. Nachtigal, M. Hansinger, M. Pfitzner, N. Chakraborty, Flame curvature distribution in high pressure turbulent bunsen premixed flames, Flow Turbul. Combust. 101 (2018) 1173–1187.
[18] M. Klein, D. Alwazzan, N. Chakraborty, A direct numerical simulation analysis of pressure variation in turbulent premixed bunsen burner flames - part 1: Scalar gradient and strain rate statistics, Comput. & Fluids 173 (2018) 178–188.
[19] N. Chakraborty, D. Alwazzan, M. Klein, R.S. Cant, On the validity of damköhler's first hypothesis in turbulent bunsen burner flames: A computational analysis, P. Combust. Inst. 37 (2019) 2231–2239.
[20] R. Rasool, N. Chakraborty, M. Klein, Effect of non-ambient pressure conditions and Lewis number variation on direct numerical simulation of turbulent bunsen flames at low turbulence intensity, Combust. Flame 231 (2021) 111500.

[21] T. Poinsot, D. Veynante, Theoretical and Numerical Combustion, second ed., R.T. Edwards, Inc., 2005.
[22] M. Klein, A. Sadiki, J. Janicka, A digital filter based generation of inflow data for spatially developing direct numerical or large eddy simulations, J. Comput. Phys. 186 (2003) 652–665.
[23] X. Gu, M. Haq, M. Lawes, R. Woolley, Laminar burning velocity and markstein lengths of methane-air mixtures, Combust. Flame 121 (1) (2000) 41–58.
[24] S. Bane, J. Ziegler, J. Shepherd, Development of one-step chemistry models for flame and ignition simulation, GALCIT Rep. GALTCITFM (2010) 53.
[25] I. Shepherd, W. Ashurst, Flame front geometry in premixed turbulent flames, Symp. (International) Combust. 24 (1) (1992) 485–491, Twenty-Fourth Symposium on Combustion.
[26] F. Creta, R. Lamioni, P.E. Lapenna, G. Troiani, Interplay of Darrieus-Landau instability and weak turbulence in premixed flame propagation, Phys. Rev. E 94 (2016) 053102.
[27] N. Chakraborty, R. Rasool, U. Ahmed, M. Klein, Relations between statistics of three-dimensional flame curvature and its two-dimensional counterpart in turbulent premixed flames, Flow Turbul. Combust. 109 (2022) 791–812.
[28] M. Matalon, B.J. Matkowsky, Flames as gasdynamic discontinuities, J. Fluid Mech. 124 (1982) 239–259.
[29] A. Lipatnikov, J. Chomiak, Molecular transport effects on turbulent flame propagation and structure, Prog. Energy Combust. Sci. 31 (1) (2005) 1–73.
[30] Ö.L. Gülder, Contribution of small scale turbulence to burning velocity of flamelets in the thin reaction zone regime, Proc. Combust. Inst. 31 (1) (2007) 1369–1375.
[31] N. Chakraborty, L. Wang, M. Klein, Streamline segment statistics of premixed flames with nonunity Lewis numbers, Phys. Rev. E 89 (2014) 033015.
[32] M. Herbert, N. Chakraborty, M. Klein, Comparison of evaluation methodologies of the fractal dimension of premixed turbulent flames in 2D and 3D using direct numerical simulation data, Flow Turbul. Combust. 113 (2024) 1145–1160.
[33] B. Mandelbrot, The Fractal Geometry of Nature, Freeman, 1983.